Scaled-particle theory analysis of cylindrical cavities in solution

Henry S. Ashbaugh

Phys. Rev. E **91**, 042315 — Published 27 April 2015

DOI: 10.1103/PhysRevE.91.042315

A Scaled-Particle Theory Analysis of Cylindrical Cavities in Solution

Henry S. Ashbaugh*

Department of Chemical and Biomolecular Engineering, Tulane University, 300 Lindy Boggs Center, New Orleans, LA 70118

* hanka@tulane.edu

Abstract

The solvation of hard, sphero-cylindrical solutes is analyzed within the context of scaled-particle theory, which takes the view that the free energy of solvating an empty, cavity-like solute is equal to the pressure-volume work required to inflate a solute from nothing to the desired size and shape within the solvent. Based on our analysis an "end cap" approximation is proposed to predict the solvation free energy as a function of the sphero-cylinder length from knowledge regarding only the solvent density in contact with a spherical solute. The framework developed is applied to extend Reiss's classic implementation of scaled-particle theory and a previously developed revised scaled-particle theory to sphero-cylindrical solutes. To test the theoretical descriptions developed molecular simulations of the solvation of infinitely long cylindrical solutes are performed. In hard-sphere solvents classic scaled-particle theory is shown to provide a reasonably accurate description of the solvent contact correlation and resulting solvation free energy per unit length of cylinders, while the revised scaled-particle theory fitted to measured values of the contact correlation provides a quantitative free energy. Applied to the Lennard-Jones solvent at a state-point along the liquid-vapor coexistence curve, however, classic scaled-particle theory fails to correctly capture the dependence of the contact correlation. Revised scaled-particle theory, on the other hand, provides a quantitative description of cylinder solvation in the Lennard-Jones solvent with a fitted interfacial free energy in good agreement with that determined for purely spherical solutes. The break down of classical scaled-particle theory does not result from the failure of the end cap approximation, however, but is indicative of neglected higher-order curvature dependencies to the solvation free energy.

Introduction

The solubility and conformation of a solute in solution is ultimately dictated by the size and shape dependence of its solvation free energy. One of the earliest molecular-based approaches used to describe the solvation of solutes of varying size is scaled-particle theory (SPT) proposed by Reiss and coworkers [1-3]. The original implementation of SPT describes the solvation of hard sphere (HS) solutes over all size scales by enforcing a smooth juncture between exact results for the dissolution of microscopic solutes and a phenomenological thermodynamic curvature expansion for the free energy of creating a macroscopic volume within the solvent. Scaled-particle theory was subsequently used to derive analytical expressions for the equation-of-state of HS fluids and the interfacial free energy of realistic and HS solvents. When applied to realistic solvents with attractive interactions and molecular topology, however, Reiss's "classic" application of SPT (cSPT) treats the solvent as effectively monatomic utilizing an empirically determined hard-sphere diameter.

Following the successes of SPT, the theory was applied to correlate the dissolution of non-polar gases in aqueous solution, where water is assumed within cSPT to be a monatomic solvent with an effective diameter of ~2.8 Å [4-6]. Stillinger demonstrated, however, that cSPT applied to hydrophobic hydration predicts a thermodynamically incorrect, non-monotonic temperature dependence of the surface tension of water displaying a maximum well above the normal boiling point [7]. Henderson furthermore showed cSPT applied to liquids near coexistence incorrectly predicts the surface tension is a decreasing function of pressure [8], while molecular simulations find the surface tension displays a maximum with increasing pressure as a result of the formation of a vapor-like layer enshrouding the solute in solvents near coexistence [9-11]. To overcome these shortcomings Stillinger incorporated the pair-correlation function,

equation-of-state, and surface tension of water in a reformulated SPT to ensure the theory conformed to the experimentally known microscopic and macroscopic limits. Following Stillinger, Ashbaugh and Pratt developed a revised SPT (rSPT) in which multi-body solvent correlations determined from simulations are used to provide an improved description of molecular-scale solvation. Revised SPT has successfully been applied to quantitatively evaluate the solvation free energy of spherical solutes in water [12] and water-like [13] solvents as well as Lennard-Jonesium [11,14] and organic solvents [15,16].

Scaled-particle theory and SPT related theories have been extended to consider fluids composed of convex bodies [17-21], random fiber networks [22], and non-monatomic, molecular solvents [15,23,24]. Application of SPT to the dissolution of non-spherical solutes, however, has been minimal. Recently a SPT treatment of sphero-cylindrical cavity-like solutes has been put forward [25], however the proposed framework employs an *ad hoc* formulation of the solute's solvent accessible volume and utilizes a polynomial expansion for the free energy over a range of solute sizes where the underlying expression diverges [26]. Hadwiger's theorem [27], on the other hand, can be used to develop a top-down, morphometric expansion of the solvation free energy of solutes of varying shape in terms of the solute volume, area, mean and Gaussian curvatures [28,29]. This morphometric approach has been used to examine the interfacial free energies of growing spherical and infinitely long cylindrical solutes in a HS fluid [30] and aqueous solutions [31]. Utilizing expansion coefficients for HS solvents determined analytically from fundamental measure theory [32], the morphometric approach has been successfully used to describe an even broader range of solute shapes, including cubes, cones, and prisms [33] as well as the colloidal depletion forces in mixtures of hard-spheres and ellipsoids [34]. The morphometric approach, however, breaks down when the solute size is comparable to the solvent

correlation length, where solvent packing and specific interactions impact solvation. This opens up the potential to build bridges between the microscopic solvation free energies derived from SPT and macroscopic morphometric approaches to develop descriptions of solvation applicable over the entire range of solute size and shape.

As a step toward extending SPT to non-spherical solute solvation, we presently examine the dissolution of sphero-cylindrical cavities in monatomic solvents. In the following section we consider the process of growing a sphero-cylindrical cavity in solution, and use our findings to develop an analytical extension of cSPT for spherical solutes to elongated sphero-cylinders. Furthermore, we extend the rSPT originally developed for spherical cavities to describe cylinder dissolution in the limit of an infinitely long cylinder. We subsequently test the application of the theoretical framework developed here using Monte Carlo simulations of two different monatomic fluids, the HS and Lennard-Jones (LJ) solvents. The HS solvent allows us to examine the impact of packing interactions, while the LJ solvent allows us to examine the impact of attractive solvent interactions on dissolution near liquid-vapor coexistence.

Theory

Cylinder Growth in Solution. The chemical potential of a hard cavity-like solute (cav) in solution formally is

$$\mu_{\text{cav}}\left(\nu\right) = kT\ln\left(\rho_{\text{cav}}\Lambda_{\text{cav}}^{3}/q_{\text{rot}}\right) - kT\ln p_{0}\left(\nu\right) \tag{1}$$

where ν is the solvent excluding volume of the cavity devoid of solvent centers, kT is the product of Boltzmann's constant and the absolute temperature, ρ_{cav} is the solute number density in solution, Λ_{cav} is the thermal de Broglie wavelength of the solute, and q_{rot} is the rotational

partition function of the solute. The quantity $p_0(\nu)$ represents the probability that a stencil of the same shape and volume of the solute randomly placed in solution is spontaneously devoid of solvent centers. The first term on the right-hand side of Eq. (1) is the ideal contribution to the chemical potential, while the second term corresponds to the excess contribution to the chemical potential resulting from molecular interactions, *i.e.*, $\mu_{\text{cav}}^{\text{ex}}(\nu) = -kT \ln p_0(\nu)$. While the ideal contribution is analytically known and independent of the solvent medium, the excess contribution is generally more complicated because it depends on multi-body correlations. While $p_0(\nu)$ is readily evaluated for solutes comparable in size to the solvent by passive observation during molecular simulations, accurate determination of this probability for larger solutes is problematic due to the increasing rarity of volume emptying fluctuations.

Rather than passive observation of solvent fluctuations, SPT takes the alternate view that the chemical potential can be obtained from the work of growing a hard solute from nothing to an empty cavity of the size and shape of interest, similar to inflating a balloon. The process of growing a sphero-cylinder into solution can be thought of as occurring in two steps (Figure 1). In the first step, a spherical cavity is grown from nothing to a solvent excluding radius *R*. In the second step, the spherical solute is extended along one axis to a length *L* from the edge of one spherical cap to the other.

The excess chemical potential for growing a spherical cavity-like solute with zero cylindrical length into solution (Figure 1, step 1) from SPT is [1]

$$\beta\mu_{\text{cav}}^{\text{ex}}(R, L=0) = kT\rho \int_0^R G(r) 4\pi r^2 \, dr . \tag{2}$$

The function $G(r)$, referred to as the contact correlation function, reports the contact values of the solute cavity-solvent radial distribution function for solute cavities with solvent-excluding radius *r*, while ρ is the solvent number density. The grouping of terms $kT\rho G(r)$ has units of pressure and $4\pi r^2\,dr$ is a differential volume element, so that Eq. (2) corresponds to the pressure-volume work to grow cavities into solution.

Extending the SPT formalism to the second step of the cylinder growth process where the initially spherical cavity is elongated along the cylindrical axis (Figure 1, step 2), the contact correlation function is replaced by the mean contact value of the cavity-solvent pair correlation function averaged over the surface of either spherical end cap of the growing cylinder. The free energy difference between the spherical and sphero-cylindrical cavities is then

$$\mu_{\text{cav}}^{\text{ex}}(R,L)-\mu_{\text{cav}}^{\text{ex}}(R,0)=kT\rho\int_0^L \overline{G}_{\text{cap}}(R,\lambda)\,\pi R^2\,d\lambda, \tag{3}$$

where $\overline{G}_{\text{cap}}(R,\lambda)$ is the mean end cap contact correlation function, which depends on the sphero-cylinder length λ but plateaus at a finite value with increasing length. A formal description of the mean contact correlation function is discussed in refs. [35,36]. For a spherical cavity that has a cylindrical length of zero, the mean end cap contact correlation function is equal to the spherical contact correlation function, *i.e.*, $\overline{G}_{\text{cap}}(R,0)=G(R)$. Summing the free energies of the first and second steps, the solvation free energy of the sphero-cylindrical cavity is

$$\mu_{\text{cav}}^{\text{ex}}(R,L)=kT\rho\int_0^R \overline{G}_{\text{cap}}(r,0)\,4\pi r^2\,dr+kT\rho\int_0^L \overline{G}_{\text{cap}}(R,\lambda)\,\pi R^2\,d\lambda \tag{4}$$

The challenge for determining the excess chemical potential of sphero-cylinder then is determining $\overline{G}_{\text{cap}}\left(R,\lambda\right)$.

If we assume $\overline{G}_{\text{cap}}\left(R,\lambda\right)$ is insensitive to the sphero-cylinder length we can equate the mean end cap contact correlation function with the contact correlation function of a sphere of the same radius, *i.e.*, $\overline{G}_{\text{cap}}\left(R,\lambda\right)\approx\overline{G}_{\text{cap}}\left(R,0\right)$, referred to here as the "end cap" approximation. Following this approximation the excess chemical potential of the sphero-cylinder is

$$\mu_{\text{cav}}^{\text{ex}}\left(R,L\right)\approx kT\rho\int_{0}^{R}\overline{G}_{\text{cap}}\left(r,0\right)4\pi r^{2}\,dr+kT\rho\overline{G}_{\text{cap}}\left(R,0\right)\pi R^{2}L \tag{5}$$

This expression notably predicts the intuitive expectation that the free energy scales as the cylinder length for sufficiently long cavities. For an infinitely long cylinder, the free energy per unit length predicted by the end cap approximation is

$$\lim_{L\to\infty}\frac{\beta\mu_{\text{cav}}^{\text{ex}}\left(R,L\right)\sigma}{L}=\rho\overline{G}_{\text{cap}}\left(R,0\right)\pi R^{2}\sigma, \tag{6}$$

where β = $1/kT$ and σ is the diameter of a solvent molecule. Following a macroscopic phenomenological thermodynamic curvature expansion, the free energy of solvating a cylinder is determined to leading order as the as the bulk pressure, *P*, times the volume plus the interfacial free energy of creating a flat interface, γ_{∞}, times the area. The resulting expansion for the free energy per unit length for an infinitely long cylinder is

$$\lim_{L\to\infty}\frac{\beta\mu_{\text{cav}}^{\text{ex}}\left(R,L\right)\sigma}{L}=\beta P\pi R^{2}\sigma+\beta\gamma_{\infty}2\pi R\sigma+order\left(R^{0}\right). \tag{7}$$

Comparing Eqs. (6) and (7), we obtain the following expansion for the contact correlation function of a spherical cavity

$$\overline{G}_{\mathrm{cap}}\left(R,0\right)=\frac{\beta P}{\rho}+\frac{2\beta\gamma_{\infty}}{\rho R}+order\left(R^{-2}\right), \tag{8}$$

which matches expectations for a macroscopic spherical cavity, giving confidence that the end cap approximation is reasonable.

While the free energy for growing a cavity into solution is independent of the path used, the mean end cap contact correlation function discussed above is only useful for evaluation of the free energy following the steps in Figure 1 in the order presented. If the sphero-cylinder is inflated from a needle of length L and radius 0 to a final radius R, then the mean contact correlation averaged over the solute surface, not just the end caps, as a function of the radius is required. For an infinitely long cylinder, the free energy per unit length can be obtained from an integral analogous to that for a spherical cavity (Eq. (2))

$$\lim_{L\to\infty}\frac{\beta\mu_{\mathrm{cav}}^{\mathrm{ex}}\left(R,L\right)\sigma}{L}=\rho\sigma\int_{0}^{R}G_{\mathrm{c}}^{\infty}\left(r\right)2\pi r\,dr, \tag{9}$$

where the cylinder contact correlation function, $G_{\mathrm{c}}^{\infty}\left(r\right)$, is the contact value of the pair-correlation function in the radial direction between an infinitely long cylinder of radius r and the solvent. The contact function is subsequently determined by the derivative

$$G_{\mathrm{c}}^{\infty}\left(R\right)=\lim_{L\to\infty}\frac{1}{2\pi\rho LR}\frac{d\beta\mu_{\mathrm{cav}}^{\mathrm{ex}}\left(R,L\right)}{dR}, \tag{10}$$

Substituting Eq. (4) into Eq. (10) and taking the appropriate limit, we obtain

$$G_{\mathrm{c}}^{\infty}\left(R\right)=\overline{G}_{\mathrm{cap}}\left(R,\infty\right)+\frac{R}{2}\frac{d\overline{G}_{\mathrm{cap}}\left(R,\infty\right)}{dR}, \tag{11}$$

which arises from the expectation that $\overline{G}_{\mathrm{cap}}\left(R,\lambda\right)$ asymptotically plateaus with increasing length. Assuming length independence we obtain

$$G_{\mathrm{c}}^{\infty}\left(R\right)\approx\overline{G}_{\mathrm{cap}}\left(R,0\right)+\frac{R}{2}\frac{d\overline{G}_{\mathrm{cap}}\left(R,0\right)}{dR}, \tag{12}$$

as the end cap approximation result for the contact correlation normal to the surface of an infinite cylinder. This expression provides a basis for assessing the accuracy of the end cap approximation by direct comparison with molecular simulation.

Classic Scaled-Particle Theory. By enforcing a smooth juncture between the known analytical limit for sub-molecular cavities and a phenomenological curvature expansion for macroscopic cavities, Reiss and coworkers derived the following cSPT expression for the solvent contact correlation function for a spherical cavity [1-3]

$$\overline{G}_{\mathrm{cap}}\left(R,0\right)=\begin{cases}\dfrac{1}{1-\eta\left(2R/\sigma_{\mathrm{s}}\right)^{3}}, & R\le\sigma_{\mathrm{s}}/2,\\[2ex] \dfrac{\beta P}{\rho}+\left[\dfrac{2+\eta}{\left(1-\eta\right)^{2}}-\dfrac{2\beta P}{\rho}\right]\left(\dfrac{\sigma_{\mathrm{s}}}{2R}\right)+\left[-\dfrac{\left(1+2\eta\right)}{\left(1-\eta\right)^{2}}+\dfrac{\beta P}{\rho}\right]\left(\dfrac{\sigma_{\mathrm{s}}}{2R}\right)^{2}, & R>\sigma_{\mathrm{s}}/2.\end{cases} \tag{13}$$

In this expression σ_{s} is the effective solvent diameter and $\eta=\pi\rho\sigma_{\mathrm{s}}^{3}/6$ is the solvent packing fraction. The effective solvent diameter is equal to the actual diameter σ of a HS solvent but is treated as an adjustable fitting parameter for solvents with more realistic interactions. This contact correlation function forms the basis of cSPT. Substituting the cSPT expression for $\overline{G}_{\mathrm{cap}}\left(R,0\right)$ into Eq. (2), the excess chemical potential of a hard-sphere cavity is

$$\beta\mu_{\mathrm{cav}}^{\mathrm{ex}}\left(R\right)=\begin{cases}-\ln\left(1-\eta\left(2R/\sigma_{\mathrm{s}}\right)^{3}\right), & R\le\sigma_{\mathrm{s}}/2,\\ \left[-\ln\left(1-\eta\right)+\dfrac{9\eta^{2}}{2\left(1-\eta\right)^{2}}-\dfrac{\eta\beta P}{\rho}\right]+\left[-\dfrac{3\eta\left(1+2\eta\right)}{\left(1-\eta\right)^{2}}+\dfrac{3\eta\beta P}{\rho}\right]\left(\dfrac{2R}{\sigma_{\mathrm{s}}}\right) & \\ \quad+\left[\dfrac{3\eta\left(2+\eta\right)}{2\left(1-\eta\right)^{2}}-\dfrac{3\eta\beta P}{\rho}\right]\left(\dfrac{2R}{\sigma_{\mathrm{s}}}\right)^{2}+\dfrac{\eta\beta P}{\rho}\left(\dfrac{2R}{\sigma_{\mathrm{s}}}\right)^{3}, & R>\sigma_{\mathrm{s}}/2.\end{cases} \tag{14}$$

Classic SPT has been used extensively to model spherical cavity dissolution in a wide range of solvents [2,4,5,15,22-24]. Recognizing for the HS solvent that a cavity of radius σ is identical to a solvent particle, the pressure can be derived by requiring self-consistency between the virial expression for the pressure, *i.e.*, $\beta P/\rho=1+4\eta\overline{G}_{\mathrm{cap}}\left(\sigma,0\right)$, and the contact correlation evaluated from Eq. (13). The HS equation-of-state derived from cSPT is [1]

$$\frac{\beta P_{\mathrm{SPT}}}{\rho}=\frac{1+\eta+\eta^{2}}{\left(1-\eta\right)^{3}}, \tag{15}$$

which is identical to that evaluated by integrating the HS compressibility determined from Percus-Yevick integral equation theory [37].

Following the end cap approximation, cSPT predicts the chemical potential of a sphero-cylindrical cavity is

$$\beta\mu_{\mathrm{cav}}^{\mathrm{ex}}\left(R,L\right)=\begin{cases}-\ln\left(1-\eta\left(2R/\sigma_{\mathrm{s}}\right)^{3}\right)+\dfrac{\left(3\eta/2\right)}{1-\eta\left(2R/\sigma_{\mathrm{s}}\right)^{3}}\left(\dfrac{2R}{\sigma_{\mathrm{s}}}\right)^{2}\left(\dfrac{L}{\sigma_{\mathrm{s}}}\right), & R\le\sigma_{\mathrm{s}}/2,\\ \left[-\ln\left(1-\eta\right)+\dfrac{9\eta^{2}}{2\left(1-\eta\right)^{2}}-\dfrac{\eta\beta P}{\rho}\right]+\left[-\dfrac{3\eta\left(1+2\eta\right)}{\left(1-\eta\right)^{2}}+\dfrac{3\eta\beta P}{\rho}\right]\left(\dfrac{2R}{\sigma_{\mathrm{s}}}\right)\\ \quad+\left[\dfrac{3\eta\left(2+\eta\right)}{2\left(1-\eta\right)^{2}}-\dfrac{3\eta\beta P}{\rho}\right]\left(\dfrac{2R}{\sigma_{\mathrm{s}}}\right)^{2}+\dfrac{\eta\beta P}{\rho}\left(\dfrac{2R}{\sigma_{\mathrm{s}}}\right)^{3} & R>\sigma_{\mathrm{s}}/2.\\ \quad+\dfrac{3\eta}{2}\left\{\begin{array}{c}\dfrac{\beta P}{\rho}\left(\dfrac{2R}{\sigma_{\mathrm{s}}}\right)^{2}+\left[\dfrac{2+\eta}{\left(1-\eta\right)^{2}}-\dfrac{2\beta P}{\rho}\right]\left(\dfrac{2R}{\sigma_{\mathrm{s}}}\right)\\ +\left[-\dfrac{\left(1+2\eta\right)}{\left(1-\eta\right)^{2}}+\dfrac{\beta P}{\rho}\right]\end{array}\right\}\left(\dfrac{L}{\sigma_{\mathrm{s}}}\right), & \end{cases} \tag{16}$$

For $R > \sigma_{\mathrm{s}}/2$ this expression conforms to the results of Benzi et al. obtained following an alternate expansion [38]. In the limit of an infinite cylinder, the chemical potential per unit length is

$$\lim_{L\to\infty}\frac{\beta\mu_{\mathrm{cav}}^{\mathrm{ex}}\left(R,L\right)\sigma_{\mathrm{s}}}{L}=\begin{cases}\dfrac{\left(3\eta/2\right)}{1-\eta\left(2R/\sigma_{\mathrm{s}}\right)^{3}}\left(\dfrac{2R}{\sigma_{\mathrm{s}}}\right)^{2}, & R\le\sigma_{\mathrm{s}}/2,\\ \dfrac{3\eta}{2}\left\{\begin{array}{c}\dfrac{\beta P}{\rho}\left(\dfrac{2R}{\sigma_{\mathrm{s}}}\right)^{2}+\left[\dfrac{2+\eta}{\left(1-\eta\right)^{2}}-\dfrac{2\beta P}{\rho}\right]\left(\dfrac{2R}{\sigma_{\mathrm{s}}}\right)\\ +\left[-\dfrac{\left(1+2\eta\right)}{\left(1-\eta\right)^{2}}+\dfrac{\beta P}{\rho}\right]\end{array}\right\}, & R>\sigma_{\mathrm{s}}/2.\end{cases} \tag{17}$$

The corresponding expression for the cylinder contact correlation function normal to the surface of an infinite cylinder is

$$G_{\mathrm{c}}^{\infty}\left(R\right)=\begin{cases}\dfrac{1+\left(\eta/2\right)\left(2R/\sigma_{\mathrm{s}}\right)^{3}}{\left[1-\eta\left(2R/\sigma_{\mathrm{s}}\right)^{3}\right]^{2}}, & R\le\sigma_{\mathrm{s}}/2,\\ \dfrac{\beta P}{\rho}+\dfrac{1}{2}\left[\dfrac{2+\eta}{\left(1-\eta\right)^{2}}-\dfrac{2\beta P}{\rho}\right]\left(\dfrac{\sigma_{\mathrm{s}}}{2R}\right), & R>\sigma_{\mathrm{s}}/2.\end{cases} \tag{18}$$

Eqs. (16) – (18) can be specialized to the hard-sphere solvent by substituting in the hard-sphere equation-of-state (Eq. (15)) in for the pressure. We note that while $G_{\mathrm{c}}^{\infty}\left(R\right)$ in Eq. (18) is continuous at $R = \sigma_{\mathrm{s}}/2$ its first derivative is not, which can potentially result in qualitative errors in the description of cylinder solvation.

In addition to predicting the equation-of-state of a HS fluid cSPT also predicts an expression for evaluating the interfacial free energy against a flat, hard interface. By comparing Eq. (18) with Eq. (8), the interfacial free energy is

$$\beta\gamma_{\infty}\sigma^{2}=\frac{3\eta}{\pi}\left[\frac{2+\eta}{2\left(1-\eta\right)^{2}}-\frac{\beta P}{\rho}\right], \tag{19}$$

which can be compared to simulation measurements of the interfacial free energy to assess the accuracy of cSPT at describing the solvation of macroscopic surfaces.

Revised Scaled-Particle Theory. When applied to solvents with realistic interactions many of the assumptions underlying the development of cSPT are more uncertain and can result in erroneous predictions, like the surface tension of water exhibits a non-monotonic dependence on temperature [7] and qualitatively incorrect shapes of the contact correlation function for organic liquids [15,23,24]. To address these difficulties, Stillinger took an empirical outlook and

built a SPT framework applied to cavities in aqueous solution that utilized the experimentally determined water oxygen pair correlations to account in part for the solvent structure in conjunction with the known interfacial free energy, bulk pressure, and density of water [7]. Following Stillinger's philosophy, we developed a revised SPT (rSPT) description of cavity solvation that combines results from molecular simulations for small cavity solvation, to account for multi-body solvent correlations, with the phenomenological curvature expansion for large cavities [12]. Revised SPT has been successfully used to describe cavity solvation in water [12], organic [15], and LJ [11,14] solvents over a range of temperatures and pressures. A full description of the development of rSPT to describe spherical cavity solvation is provided in Refs. [11,12,14,15]. Here we describe the application of rSPT to infinitely long cylindrical cavities.

Revised SPT describes cavity solvation from microscopic to macroscopic radii by smoothly interpolating the excess chemical potential between values directly determined from particle insertion averages evaluated from simulations for microscopic cavities and the thermodynamic curvature expansion for macroscopic cavities. For an infinitely long cylindrical cavity, the excess chemical potential per unit length as described by rSPT is

$$\lim_{L\to\infty} \frac{\beta\mu_{\mathrm{cav}}^{\mathrm{ex}}\left(R,L\right)\sigma}{L} = -\ln p_0^{\infty}\left(R\right) f\left(R\right) + \Gamma\left(R\right)\left[1 - f\left(R\right)\right]. \tag{20}$$

In this expression, $f(R)$ is a switching function equal to 1 below R_{sim} and 0 above R_{macro} that smoothly interpolates between these two bounds. We adopt a cubic form for the function $f\left(R\right)$ that smoothly switches the simulation and macroscopic chemical potentials between R_{sim} and R_{macro},

$$f\left(R\right)=\begin{cases} 1, & R<R_{\text{sim}}, \\ 1-3\dfrac{\left(R-R_{\text{sim}}\right)^{2}}{\left(R_{\text{macro}}-R_{\text{sim}}\right)^{2}}+2\dfrac{\left(R-R_{\text{sim}}\right)^{3}}{\left(R_{\text{macro}}-R_{\text{sim}}\right)^{3}}, & R_{\text{sim}}\le R\le R_{\text{macro}}, \\ 0, & R>R_{\text{macro}}. \end{cases} \tag{21}$$

The probability $p_0^{\infty}\left(R\right)$ in Eq. (20), evaluated from molecular simulations for microscopic cavities, represents the infinite cylinder length limit of the cylinder insertion probability raised to the power of σ/L, *i.e.*, $p_0^{\infty}\left(R\right)=\lim_{L\to\infty}p_0\left(R,L\right)^{\sigma/L}$. While $p_0\left(R,L\to\infty\right)$ is zero for a cylinder of any radius greater than zero, since cavity overlap with one or more solvent molecules is guaranteed in this limit, the free energy of cavity solvation is expected to be proportional to the cylinder length with increasing size. Resultantly, $p_0\left(R,L\right)$ is expected to exponentially decay to zero with increasing cylinder length so that $p_0^{\infty}\left(R\right)$ is a well-defined function of radius alone. The remaining function in Eq. (20), $\Gamma(R)$, represents the macroscopic curvature expansion for excess chemical potential given as

$$\Gamma\left(R\right)=\beta P\pi\sigma R^{2}+\beta\gamma_{\infty}2\pi\sigma R+\beta\lambda 2\pi\sigma-\frac{\beta\omega 2\pi\sigma}{R}-\frac{\beta\varphi\pi\sigma}{R^{2}}. \tag{22}$$

We truncate this expression after order R^{-2} contributions where molecular packing and specific correlations are assumed to dominate. As above, P is the bulk solvent pressure, γ_{∞} is the interfacial free energy for creating a hard, flat surface in the solvent, while λ, ω, and φ are higher-order contributions in a curvature expansion of the free energy.

For cavities larger than the solvent, the contact correlation function is readily accessible by direct simulation of an explicit hard cylinder in solution. In this case, rSPT is more accurately applied by fitting to simulation contact values rather than the chemical potential as implied by

Eq. (20). By differentiating Eq. (20) with respect to R, the rSPT expression for the contact correlation function is

$$G_{\mathrm{c}}^{\infty}\left(R\right)=-\frac{f\left(R\right)}{2\pi\rho\sigma R}\frac{\partial\ln p_0^{\infty}\left(R\right)}{\partial R}-\frac{\ln p_0^{\infty}\left(R\right)}{2\pi\rho\sigma R}\frac{\partial f\left(R\right)}{\partial R}+\left(\frac{\beta P}{\rho}+\frac{\beta\gamma_{\infty}}{\rho R}+\frac{\beta\omega}{\rho R^3}+\frac{\beta\varphi}{\rho R^4}\right)\left[1-f\left(R\right)\right]$$

$$-\left(\frac{\beta PR}{2\rho}+\frac{\beta\gamma_{\infty}}{\rho}+\frac{\beta\lambda}{\rho R}-\frac{\beta\omega}{\rho R^2}-\frac{\beta\varphi}{2\rho R^3}\right)\frac{\partial f\left(R\right)}{\partial R}. \tag{23}$$

The range of cavity radii for which $G_{\mathrm{c}}^{\infty}\left(R\right)$ can be accurately determined from cavity insertion and smoothly knit together with the phenomenological macroscopic expansion determines the switching bounds R_{sim} and R_{macro}. While the solvent density and pressure are taken from the bulk solvent simulations, the remaining parameters γ_{∞}, λ, ω, and φ are obtained from a least squares fit to the solvated cylinder simulation results.

Simulation Details

To examine the application of SPT to cylindrical cavity solvation we have performed simulations of the HS and LJ solvents. In the case of the HS fluid we considered densities ranging from gas to liquid-like, while for the LJ fluid we examined a single liquid state point close to vapor-liquid coexistence. In addition to simulations of cylindrical cavities we have also modeled spherical cavities in a HS solvent in order to test the accuracy of the end cap approximation. In the case of spherical cavities in the LJ solvent, we use results we previously reported in the Ref. [14]. Below we describe the series of simulations conducted for each system.

For the HS fluid, four different sets of grand canonical Monte Carlo simulations [39] were performed to evaluate averages required to fit rSPT to contact correlations for both spherical and cylindrical cavities. Simulations were performed with the solvent chemical

potential adjusted so that the nominal average bulk density is $\rho\sigma^3$ = 0.1, 0.2, 0.3, 0.4, 0.5, 0.6, 0.7, 0.8, and 0.85. In the first two sets of simulations, the pure solvent was simulated to evaluate spherical and cylindrical cavity insertion probabilities, $p_0\left(R\right)$ and $p_0^\infty\left(R\right)$, respectively. To evaluate spherical cavity insertion probabilities, a periodic cubic cell 10σ in length on a side was simulated. Following at least 10^9 solvent insertion, deletion, and translational moves within the grand canonical ensemble for equilibration, a total of $5\text{x}10^9$ solvent insertion, deletion, and translational moves were performed for evaluation of thermodynamic averages. Spherical cavity insertion probabilities were periodically evaluated by attempting 2000 random insertions following every 25,000 grand canonical moves.

Evaluation of cavity insertion probabilities is more challenging for an infinitely long cylindrical cavity since an infinite number of solvent centers can fit within a cylinder of finite radius, leading to a zero probability of insertion. As noted above, however, $p_0^\infty\left(R\right) \approx p_0\left(R,L\right)^{\sigma/L}$ is expected to be finite in the infinite length limit. To evaluate $p_0\left(R,L\right)^{\sigma/L}$ we have performed simulations of cubic cells 6σ and 8σ in length on a side. Grand canonical simulations were conducted for the same equilibration and production lengths as for the spherical cavities. Similarly, 2000 infinite cylindrical cavity insertions were attempted every 25,000 grand canonical moves. For each insertion attempt we randomly selected the *x*-, *y*-, or *z*-axis to align the cylinder and randomly choose a point on the plane normal to the alignment axis to center the cavity. Within the simulation errors we found quantitative agreement between the probabilities $p_0\left(R,L\right)^{\sigma/L}$ obtained for the 6σ and 8σ simulation box sizes, giving confidence our estimates of

the infinite cylinder limit, *i.e.*, $p_0^{\infty}\left(R\right)$, are accurate. We subsequently used our results for the 6σ box for rSPT analysis.

In a second set of simulations, we determined contact correlation functions at discrete cavity radii by direct simulation of explicit spherical and cylindrical cavities solvated in the HS solvent. Grand canonical Monte Carlo simulations were performed at the same densities listed in for the insertion simulations above. Explicit spherical and cylindrical cavity solvent excluding radii of 0.25σ, 0.5σ, 0.75σ, 1σ, 1.5σ, 2σ, 2.5σ, 3σ, 3.5σ, 4σ, 4.5σ, and 5σ were simulated. The cylindrical cavities were aligned along the *x*-axis of the simulation box to model an infinite rod. For the spherical cavity simulations, the cell side length was set to the cavity diameter plus 12σ to provide a buffer between the periodic images. For the cylindrical cavity, the box length in the *x*-direction along the cylinder length was 10σ, while the box length in the *y*- and *z*-directions was set to the cylinder diameter plus 16σ. For both the spherical and cylindrical cavities, the simulations were equilibrated by performing at least 10^9 solvent insertion, deletion, and translational moves. Following equilibration, 10^{10} solvent insertion, deletion, and translational moves were performed for evaluation of thermodynamic averages.

To examine the effects of solvent attractions we performed simulations of cylindrical cavities in a LJ solvent near coexistence where attractions are expected to play a significant role. Following the HS simulations, we performed two sets of simulations with and without the cavity explicitly included to evaluate the averages required to fit rSPT. We have previously performed extensive simulations of spherical cavities in the LJ solvent [14], so here we only performed simulations of cylindrical cavity solvation. The LJ solvent was modeled using the cut-shifted interaction

$$\varphi_{\text{cut}}(r)=\begin{cases}\varphi_{\text{LJ}}(r)-\varphi_{\text{LJ}}(r_{\text{c}}), & r<r_{\text{c}},\\ 0, & r\geq r_{\text{c}},\end{cases} \tag{24}$$

with no long range interaction corrections. In this expression $\varphi_{\text{LJ}}(r)=4\varepsilon\left(\sigma^{12}/r^{12}-\sigma^{6}/r^{6}\right)$ is the full interaction, ε and σ in the context of the LJ solvent are the well-depth and diameter, respectively, and $r_{\text{c}} = 2.5\sigma$ is the LJ interaction cut-off separation. Our simulations in the LJ fluid were performed in the grand canonical ensemble at a temperature of $kT/\varepsilon = 0.85$ with the chemical potential adjusted to give a liquid density of $\rho\sigma^3 = 0.70$ and a corresponding pressure of $P\varepsilon/\sigma^3 = 0.023$, which we previously found lies just above the solvent vapor pressure at this temperature [14]. Additional state points were not considered since these simulations take considerably longer than the HS solvent owing to the range of the LJ potential.

To determine the cylindrical cavity insertion probabilities the same simulation procedures as for the HS solvent described above were used, with the same box sizes to check the accuracy of our estimate for the infinite cylinder length limit. For the second set of simulations, an explicit cylindrical cavity was included in the simulation box to directly determine the solvent contact densities. For the cylindrical cavity, the box length in the *x*-direction along the cylinder length was 10σ, while the box length in the *y*- and *z*-directions was set to the cylinder diameter plus 12σ. Explicit cylindrical cavity radii of 0.25σ, 0.5σ, 0.75σ, 1σ, 1.5σ, 2σ, 2.5σ, 3σ, 3.5σ, 4σ, 4.5σ, and 5σ were examined. These simulations were equilibrated by performing at least 10^9 solvent insertion, deletion, and translational moves. Following equilibration, 10^{10} solvent insertion, deletion, and translational moves were performed for evaluation of thermodynamic averages.

Results and Discussion

Hard-Sphere Solvent. The contact correlation's of a HS solvent at $\rho\sigma^3 = 0.8$ in contact with a spherical cavity and an infinitely long cylindrical cavity as a function of their radii is reported in Figure 2. The contact correlation determined by explicit simulation of solute cavities show the contact density monotonically grows with radius for both the spherical and cylindrical cavities. The growth of the contact correlations appear to approach an asymptotic plateau with increasing radius, consistent with the expected contact density for a flat interface of $\beta P/\rho = 7.75$ (Table 1) as dictated by the wall theorem [40]. Compared against the spherical solute the cylinder's contact correlation grows more quickly with increasing radius. This difference can be rationalized in terms of the lower curvature of a cylinder ($1/R$) that is closer to a flat surface compared to the curvature of a sphere ($2/R$). Classic SPT qualitatively captures the spherical and cylindrical contact correlations, although the contact values are generally greater than that observed from simulation (Figure 2). This over prediction of the contact value reflects the over prediction of the pressure by Eq. (15) (Table 1), ultimately giving rise to a larger predicted contact value of the HS density at a flat wall. Spherical rSPT on the other hand provides an excellent quantitative description of the contact correlation of the HS solvent solvating a spherical cavity (Figure 2), in agreement with previous studies of spherical cavity solvation in water [12], hexane [15], and the LJ liquid [11,14]. Utilizing the rSPT fit to the spherical cavity we can predict the contact correlation of the cylinder using the end cap approximation (Eq. (12)). As can be seen in Figure 2 the end cap approximation provides an excellent quantitative prediction of the radial contact correlation of the cylindrical cavity.

End cap approximation predictions of the cylinder contact correlation as a function of the HS solvent density utilizing rSPT fits to spherical cavity contact correlation are excellent (Figure

3a). The largest discrepancy between the predicted contact correlations and those observed by direct simulation is found for cylindrical cavities of radius 0.25σ. Revised SPT applied to cylindrical cavities overcomes this discrepancy, however, by incorporating small radii insertion results from simulation into fits of Eq. (23) to the explicit simulation contact values (Figure 3b). The differences between simulation, the rSPT fits, and end cap predictions for small cavities ($R < 0.5\sigma$) are more clearly observed when $G_{\mathrm{c}}^{\infty}\left(R\right)-1$ is plotted versus radius on a log-log scale (Figure 4). While rSPT accurately describes the contact correlation, the end cap approximation under predicts the contact values for radii less than ~0.5σ. More importantly we observe a steeper slope on the logarithmic scale for the end cap approximation than observed from the cylindrical rSPT fit, indicating this approximation over predicts the scaling exponent of the dependence of the contact correlation on radius.

To derive an approximate form for $G_{\mathrm{c}}^{\infty}\left(R\right)$ in the small radius limit we consider a permeable cylindrical observation volume embedded within the solvent under periodic boundary conditions, analogous to the simulations used to determine small cylinder insertion probabilities for rSPT. As the observation cylinder's radius approaches zero we assume that the maximum number of solvent centers observed within the volume is two, although multiple solvent centers may potentially fit in principle. The probability p_i of observing i = 0, 1, or 2 solvent centers within the observation volume satisfy the equations [41]

$$p_0 + p_1 + p_2 = 1, \tag{25a}$$

$$p_1 + 2p_2 = \left\langle n \right\rangle = \rho\pi R^2 L, \tag{25b}$$

$$p_1 + 4p_2 = \left\langle n^2 \right\rangle = \rho\pi R^2 L + \rho^2 \iint_V g\left(\left|\boldsymbol{r}-\boldsymbol{r}'\right|\right) d\boldsymbol{r}\, d\boldsymbol{r}', \tag{25c}$$

where n indicates the number of solvent centers within the observation volume ($V = \pi R^2 L$) at any instant, and $g(r)$ is the solvent radial distribution function. Assuming the solvent radial distribution function is described by the low density HS radial distribution function (a step function jumping from 0 to 1 at $r = \sigma$) and the integral in Eq. (25c) can be treated as psuedo one-dimensional for small radii cylinders, the mean square number of solvent centers is approximately

$$\left\langle n^2 \right\rangle \approx \rho\pi R^2 L + \rho^2 \pi^2 R^4 L^2 - 2\rho^2 \sigma \pi^2 R^4 L \tag{26}$$

The probability the solute observation volume is empty is subsequently given as

$$p_0(R,L) = 1 - \rho\pi R^2 L + \frac{\rho^2 \pi^2 R^4 L^2}{2} - \rho^2 \sigma \pi^2 R^4 L. \tag{27}$$

Substituting Eq. (27) into Eq. (10) and expanding in terms of the cylinder radius, the leading contribution to order R^2 of the contact correlation is

$$G_c^{\infty}(R \to 0) \approx 1 + 2\rho\sigma\pi R^2 + order\left(R^4\right). \tag{28}$$

The contact correlation is thereby expected to grow as the radius squared in the small radius limit, while the end cap approximation predicts a cubic dependence, *e.g.*, Eq. (18). This difference reflects the differing dependence of the volume of a cylinder and sphere on radius. We note that while assuming only one solvent particle at most is found within the observation volume in the small radius limit, *i.e.,* $p_0(R,L) = 1 - \rho\pi R^2 L$, yields the correct contact value of one when the radius is zero, the R^2 contribution to G_c^{∞} also includes cylindrical length contributions that diverge in the infinite cylinder limit. Incorporation of pair correlations (Eq. (26)), albeit in an approximate manner, permits evaluation of the leading order dependence of the contact correlation on the cylinder radius, however, the higher order terms (R^4 and above)

diverge. It may be surmised that increasing orders of multi-body correlations must be utilized to evaluate higher order radial contributions, attributable to the fact that an infinite number of solvent molecules can fit within an infinitely long cylinder with a non-zero radius.

Despite the approximations made, Eq. (28) provides a significantly improved prediction of the contact correlation in the small radius limit compared to the end cap approximation (Figure 4). For the lowest density simulated ($\rho\sigma^3 = 0.1$) Eq. (28) provides a nearly quantitative prediction of the contact correlation up to $R = 0.5\sigma$, reflecting the accuracy of the assumptions underlying Eqs. (25) and (26) at low density. Even at the highest density simulated Eq. (28) provides a semi-quantitative description of the small radius contact correlation. More importantly, Eq. (28) more accurately captures the contact correlation small radius scaling behavior than predicted by the end cap approximation, providing physical insights into the short comings of the end cap approximation for small radii cylinders.

The interfacial tension for creating flat interface in the HS solvent obtained by fitting rSPT to either the cylindrical or spherical cavity contact densities are in excellent agreement with each other over the entire range of densities simulated (Figure 5 and Table 1). Moreover, our results generally agree with those obtained from HS simulations following alternate thermodynamic routes [42-44]. Despite the fact that cSPT over predicts the contact correlation for both spherical and cylindrical cavities, the cSPT interfacial tension prediction (Eq. (19)) is in excellent agreement with the rSPT fits (Figure 5 and Table 1), differing by less than 1% at the highest densities simulated. At densities approaching HS freezing ($\rho\sigma^3 \approx 0.94$) Eq. (19) is known to become more inaccurate [44].

The excess solvation free energy per unit length for cylindrical cavities in HS solvents is readily obtained by integrating the contact correlations described above using Eq. (9). The free

energy for cylinders at a solvent density of $\rho\sigma^3 = 0.8$ is reported in Figure 6. The free energies obtained depend approximately quadratically on the cylinder radius. This dependence results from the dominance of the macroscopic pressure contribution to the free energy ($\beta P/\rho = 7.75$ at this state point as noted above, significantly greater than the ideal gas pressure or a liquid near vapor coexistence), even for cavities with radii less than 3σ. Given the accuracy of rSPT at reproducing the cylinder contact correlations (Figure 3b), rSPT is expected to provide the most accurate quantitative value of the cylinder solvation free energy. The free energy obtained from the end cap approximation is in near perfect agreement with that obtained from rSPT, differing by less than 0.02% at $R = 3\sigma$. Classic SPT, on the other hand over predicts the rSPT free energy by 4.8% at $R = 3\sigma$. This difference reflects cSPT's over prediction of the HS solvent pressure (Table 1), which could be alleviated by substituting the simulation pressure or a more accurate HS equation of state in the expression for the contact correlation. Substitution of pressures differing from Eq. (15), however, can lead to discrepancies in the predicted interfacial free energy and solvation properties of solvent-sized and smaller cavities.

Lennard-Jones Solvent near Coexistence. The rSPT fit to simulation values of the contact correlation for infinitely long cylinders in a LJ solvent at $kT/\varepsilon = 0.85$ and $P\sigma^3/\varepsilon = 0.023$, close to liquid-vapor coexistence, is reported in Figure 7a. The overall fit is excellent over the range of cylinder radii simulated, giving further confidence in the utility of rSPT applied to a range of solvents. In difference to the HS solvent, the cylinder contact correlation function in the LJ solvent exhibits a maximum at a radius just slightly greater than $\sigma/2$. Following the maximum the contact correlation rapidly falls to values below one at radii comparable to the solvent diameter, indicative of a vapor-like layer surrounding the cylinder. With growing radial size the

contact density is expected to asymptotically approach the bulk compressibility factor for the saturated liquid ($\beta P/\rho$ = 0.0387), which is necessarily less than the bulk liquid density as a result of condensed phase attractions that nearly perfectly balance the ideal gas contribution to the pressure along the saturation curve. The interfacial free energy obtained from fitting rSPT to cylinder contact densities is in good agreement with that we obtained previously fitting to spherical cavities (Table 1) [14], differing by only 5%. The surface tension of the LJ solvent is positive in difference to the hard sphere solvent, which is manifested as the decay in the contact correlation function to the bulk compressibility limit for the LJ solvent (Figure 7a) rather than the monotonic rise towards the limit observed for the HS solvent (Figure 2).

While cSPT provides a reasonable semi-quantitative description of cylinder solvation in the HS solvent, its description of the cylinder contact correlation function in the LJ solvent is problematic (Figure 7b). Classic SPT using an effective diameter of $\sigma_s = 1\sigma$ significantly over predicts the contact densities observed for cylinders of increasing size, resulting from a significant over prediction by more than a factor of 2 of the interfacial free energy (Table 1). Moreover, cSPT applied to cylinder solvation predicts a sharp cusp at the maximum in the contact correlation for cavities with a radius of $R = \sigma_s/2$. While the approximations used to extend cSPT from spherical to cylindrical cavities maintain continuity of the contact correlation function at the joining point between the microscopic and macroscopic descriptions of solvation, they do not enforce continuity of the first derivative of the contact correlation required to ensure a smooth function. This results in the cusp observed for cavity solvation in the LJ solvent. A discontinuity in the first derivative of the cSPT prediction for the contact correlation function occurs at the joining point for the HS solvent as well, but since the contact correlation in the HS solvent is monotonically increasing over all cylinder radii the discontinuity is not readily

observed by eye (Figure 2). If we fit the effective cSPT solvent diameter to the interfacial tension obtained from rSPT (Table 1) we obtain an unphysically low value of $\sigma_s = 0.792\sigma$, well inside the excluded volume of any individual solvent particle. The cylinder contact correlation function predicted by cSPT using the fitted solvent diameter accurately tracks the rSPT result for radii greater than 2σ (Figure 7b), which is not surprising given that the fitted diameter brings cSPT into conformity with the expected macroscopic radial dependence. For molecular scale cylinders with radii less than 2σ, however, the fitted cSPT under predicts $G_c^{\infty}\left(R<2\sigma\right)$ while retaining the joining cusp.

The end cap approximation provides an improved prediction of $G_c^{\infty}\left(R\right)$ utilizing the contact correlation function previously obtained from rSPT applied to spherical cavities (Figure 7a) over cSPT [14]. Specifically, the end cap approximation is in near quantitative agreement with the cylindrical rSPT fit for radii greater than 1σ. For radii near 0.5σ the end cap approximation over predicts the contact density by ~30%. More importantly, the end cap approximation predicts $G_c^{\infty}\left(R\right)$ is smooth with a maximum near 0.5σ, in qualitative agreement with the cylindrical rSPT fit. An interesting consequence of the end cap approximation (Eq. (12)) is that the predicted $G_c^{\infty}\left(R\right)$ will intersect $\overline{G}_{\text{cap}}\left(R,0\right)$ at the radius for which $\overline{G}_{\text{cap}}\left(R,0\right)$ is a maximum. Comparing the cylindrical and spherical rSPT contact correlation fits to simulation, however, this prediction is incorrect (Figure 7a).

The cylinder excess solvation free energies per unit length in the LJ solvent determined by integrating the cylinder contact correlation is reported in Figure 8. Along the saturation curve the pressure of the LJ solvent is considerably less than that in the HS solvent. For the cavity radii reported in this figure ($R < 3\sigma$) then, interfacial rather than pressure effects dominate the free

energy. As a result the solvation free energy is effectively linear with radius for cylinders just larger than the solvent diameter, with a magnitude significantly less than that reported for the HS solvent (Figure 6). Using an effective solvent diameter of 1σ cSPT predicts too strong a dependence of the free energy on radius compared to rSPT. While cSPT correctly reproduces changes in the free energy with changes in cylinder radii for sizes greater than ~1.5σ using the fitted solvent diameter of 0.792σ, the absolute free energy measured relative to a cavity radius of zero is under predicted by a constant difference of $\Delta\beta\mu_{\text{cav}}^{\text{ex}}\sigma / L$ = -2.4. These trends follow from the over predicted interfacial free energy using $\sigma_s = 1\sigma$ (Table 1) and the under predicted contact structure for molecular sized cavities using $\sigma_s = 0.792\sigma$ (Figure 7b). The end cap approximation, on the other hand, provides a significantly improved prediction of the cylinder free energy over the entire range of cylinder sizes reported in Figure 8, differing only by a smaller constant difference of $\Delta\beta\mu_{\text{cav}}^{\text{ex}}\sigma / L$ = 0.9 for radii lager than 1σ. The superior prediction of the end cap approximation over cSPT using the fitted solvent diameter, in turn, can be traced to the improved description of the cylinder contact correlation and incorporation of higher order curvature contributions (Figure 7a).

Conclusions

We have presented a detailed analysis of the solvation of hard sphero-cylinder solutes over a range of densities in the case of the HS fluid and at a single liquid state point close to liquid-vapor coexistence in the case of the LJ fluid. Three SPT based approaches were developed to describe cylinder solvation: An analytical approach founded on the cSPT originally developed by Reiss and coworkers; an extension of the rSPT we previously developed to correlate radial solvent contact densities about an infinitely long cylindrical solute; and a physically grounded

approximation, referred to as the end cap approximation, that extends results for spherical solutes to sphero-cylinders of any desired length. Results from these three approaches were compared against molecular simulations of infinitely long cylinders. Fitting of rSPT was shown to quantitatively describe the cylindrical contact correlations observed from simulation, yielding accurate interfacial free energies consistent with results obtained from spherical solutes and following an alternate thermodynamic approaches. As such, free energies obtained from rSPT can be considered quantitatively accurate. Nevertheless, the cylinder rSPT expression developed here only applies to infinitely long cylinders. The cSPT and end cap predictions, on the other hand can be applied to sphero-cylinders of finite length. Comparing the predictions of cSPT to infinitely long cylinders against rSPT fits, cSPT was found to over estimate the free energy of cylinders in HS fluids as a result of the over estimation of the solvent pressure. In the case of the LJ solvent, cSPT predicts physically unrealistic cusps in the solvent contact correlation that cannot be alleviated even when the effective solvent diameter is considered an adjustable parameter. The end cap approximation on the other hand provides essentially quantitative agreement for the solvation free energy of cylinders in both solvents. The contact correlations predicted by the end cap approximation, moreover, were more physically reasonable than those predicted by cSPT with improved quantitative agreement over a wider range of cylinder radii. The end cap approximation subsequently can be thought of as an accurate, predictive bridge between spherical and sphero-cylindrical cavity solutes.

Acknowledgements

The work presented here has benefited from a number of fruitful conversations with Prof. Lawrence Pratt regarding solution thermodynamics and the application of scaled-particle theory

to non-spherical solutes. Financial support from the National Science Foundation under an NSF-CAREER award (CTS-0746955) and NSF-EPSCoR Cooperative Agreement No. EPS-1003897 with additional support from the Louisiana Board of Regents is gratefully acknowledged.

Table 1. Compressibility factor ($\beta\Pi/\rho$) and interfacial free energy ($\beta\gamma_\infty\sigma^2$) for creating a flat interface against a hard surface for the simulated systems. The first column reports the simulation densities. The second and third columns report the compressibility factors determined from simulation and cSPT (Eq. (15)). The fourth and fifth columns report the interfacial free energies determined from fits of rSPT to cylindrical and spherical geometries, while the final column reports the interfacial free energy predicted by cSPT (Eq. (19)). The top rows report results for the HS solvent and the final row reports results for the LJ solvent. The numbers in parentheses identify the simulation error in the last reported digit.

	$\beta\Pi/\rho$		$\beta\gamma_\infty\sigma^2$		
$\rho\sigma^3$	simulation	cSPT	cylinder	sphere	cSPT*
HS solvent					
0.100	1.24268(5)	1.23989	-0.0056(2)	-0.0055(1)	-0.0049
0.200	1.5501(2)	1.5547	-0.0223(5)	-0.0220(3)	-0.0242
0.300	1.9635(4)	1.9724	-0.0650(4)	-0.661(7)	-0.0682
0.400	2.5187(1)	2.5341	-0.1550(7)	-0.1547(9)	-0.1534
0.499	3.2642(3)	3.3011	-0.309(1)	-0.312(2)	-0.3066
0.599	4.2871(3)	4.3686	-0.572(2)	-0.579(1)	-0.5729
0.699	5.7140(2)	5.8859	-1.012(2)	-1.024(2)	-1.0285
0.799	7.7501(4)	8.0926	-1.74(3)	-1.767(5)	-1.8052
0.848	9.086(1)	9.563	-2.38(8)	-2.357(9)	-2.3783
LJ solvent ($kT/\varepsilon = 0.85$)					
0.700	0.0387(2)	N/A	0.441(5)	0.419(7)	1.0169

* $\sigma_s = 1\sigma$ for all calculations presented in this column.

Figure Captions

Figure 1. Sphero-cylindrical cavity scaled-particle theory growth scheme. In the first step, an empty spherical cavity is grown in solvent from nothing to a final radius R. The variable r measures the intermediate radius of the growing cavity from 0 to R in Eq. (1). In the second step, the spherical cavity is elongated along the central cylindrical axis to a final length of L. The variable λ measures the intermediate length of the extending sphero-cylinder from 0 to L in Eq. (3). The shaded end of the sphero-cylinder indicates the region over which the contact correlation function is averaged to determine the mean end cap contact correlation function, $\overline{G}_{\text{cap}}\left(R,\lambda\right)$, used in Eq. (3).

Figure 2. (Color online) Comparison of the contact correlation for a HS solvent against spherical and infinitely long cylindrical cavities at a density of $\rho\sigma^3$ = 0.8. Results are reported for simulations, cSPT (Eqs. (13) and (18)), fit of spherical rSPT to the spherical cavity simulations [11,14], and predictions of the cylindrical contact correlation using the end cap approximation (Eq. (12)). The symbols are identified in the figure caption. Simulation error bars are smaller than the symbols. The spherical rSPT fit used cubic switching function (Eq. (21)) parameters of $R_{\text{sim}} = 0.75\sigma$ and $R_{\text{macro}} = 1\sigma$.

Figure 3. (Color online) Contact correlations for a hard sphere solvent against an infinitely long cylindrical cavity as different densities. The solvent densities reported are $\rho\sigma^3$ = 0.1, 0.3, 0.5, 0.7 and 0.85, with the direction of increasing density indicated by the red arrow. The filled circles indicate simulation results. Simulation error bars are smaller than the symbols. The lines

indicate: **a**) Predictions of the end cap approximation (Eq. (12)) using rSPT contact correlations fitted to spherical cavity simulations; and **b**) Fits of the cylindrical rSPT (Eq. (23)) to the simulation results. The blue arrow in **a** indicates the small radius region where the end cap approximation under predicts the contact correlation. The spherical rSPT fits used cubic switching function (Eq. (21)) parameters of $R_{sim} = 0.75\sigma$ and $R_{macro} = 1\sigma$, while the cylindrical rSPT fits used $R_{sim} = 0.4\sigma$ and $R_{macro} = 0.65\sigma$.

Figure 4. (Color online) Small radius behavior of the cylindrical contact correlation of an infinitely long cylinder with a HS solvent. The results in **a** and **b** indicate results obtained at densities of $\rho\sigma^3 = 0.1$ and 0.85, respectively. Results are reported from simulation of explicit cylinders in solution, fits of the cylindrical rSPT (Eq. (23)) to the simulation results, predictions of the end cap approximation (Eq. (12)), and the low density probability expansion (Eq. (28)). The symbols are identified in the figure caption.

Figure 5. (Color online) Surface tension of a hard sphere solvent as a function of the fluid density. Results from cSPT (Eq. (19)) and fits of rSPT to both spherical and cylindrical contact correlations from simulation are reported. Data are reported in Table 1. The symbols are identified in the figure caption. Revised SPT fit error bars are smaller than the symbols.

Figure 6. (Color online) Solvation free energy per unit length of an infinitely long cylindrical cavity in a HS solvent at $\rho\sigma^3 = 0.8$. Results are reported for cSPT (Eq. (17)), the end cap approximation, and cylinder rSPT. The end cap and cylinder rSPT results are obtained by

substituting the contact correlations analogous to those reported in Figure 3a and 3b, respectively, into Eq. (9). The symbols are identified in the figure caption.

Figure 7. (Color online) Comparison of the contact correlation for a LJ solvent against spherical and infinitely long cylindrical cavities. The solvent is at a reduced temperature of $kT/\varepsilon = 0.85$ and pressure of $P\sigma^3/\varepsilon = 0.023$ ($\rho\sigma^3 = 0.699$), which lies on the liquid side of the liquid-vapor coexistence curve. **a**) Results are presented for the contact correlation from simulations of an explicit cylinder, the cylinder rSPT fit (Eq. (23)) to the simulation results, previously reported spherical rSPT in Ref. [14], and predictions of the end cap approximation using the spherical rSPT contact correlation (Eq. (12)). **b**) Comparison of the cylinder rSPT fit in **a** against cSPT predictions (Eq. (18)) obtained for $\sigma_s = 1\sigma$ and 0.792σ. The symbols are identified in the figure caption. The cylindrical rSPT fit used cubic switching function (Eq. (21)) parameters $R_{sim} = 0.4\sigma$ and $R_{macro} = 0.65\sigma$. While the rSPT fit was carried out to a maximum simulated cavity radius of 5σ we only show results up to 3σ here to more clearly view the results for smaller radius solutes.

Figure 8. (Color online) Solvation free energy per unit length of an infinitely long cylindrical cavity in a LJ liquid at $kT/\varepsilon = 0.85$ and $P\sigma^3/\varepsilon = 0.023$. Results are reported from the cylinder rSPT fit to the simulation results, predicted from the end cap approximation, and cSPT using $\sigma_s = 1\sigma$ and 0.792σ (Eq. (17)).

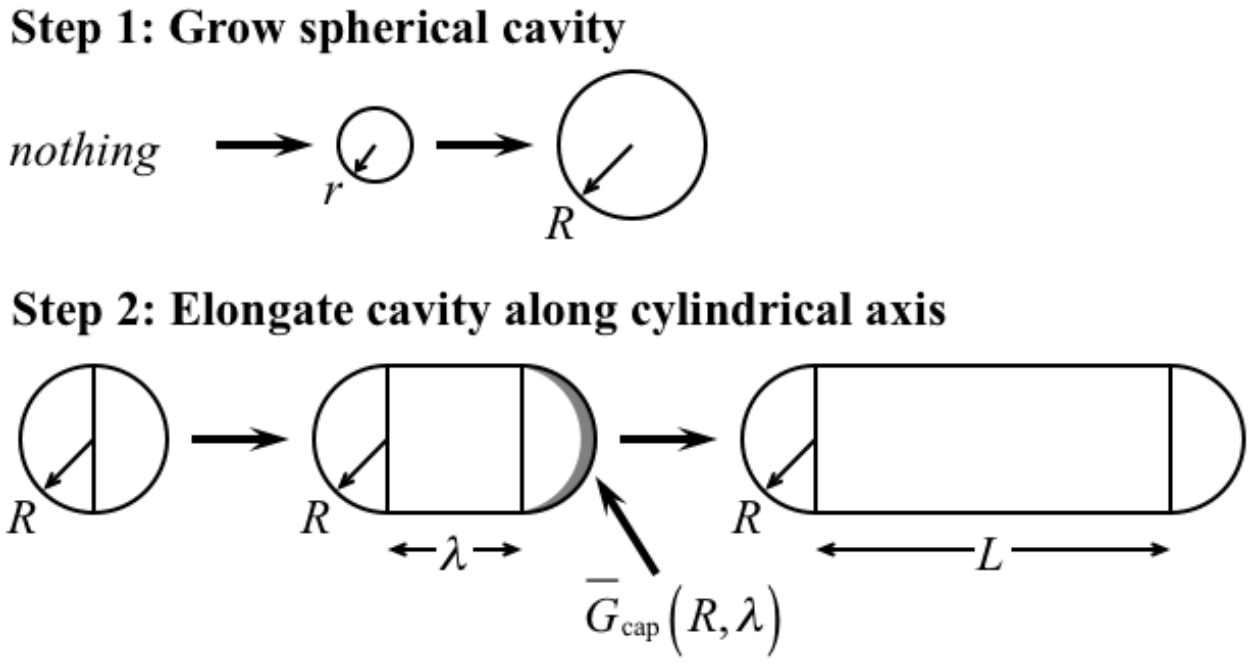
Step 1: Grow spherical cavity
nothing
r
R
Step 2: Elongate cavity along cylindrical axis
R
R
λ
R
L
$\overline{G}_{\text{cap}}(R,\lambda)$

Figure 1.

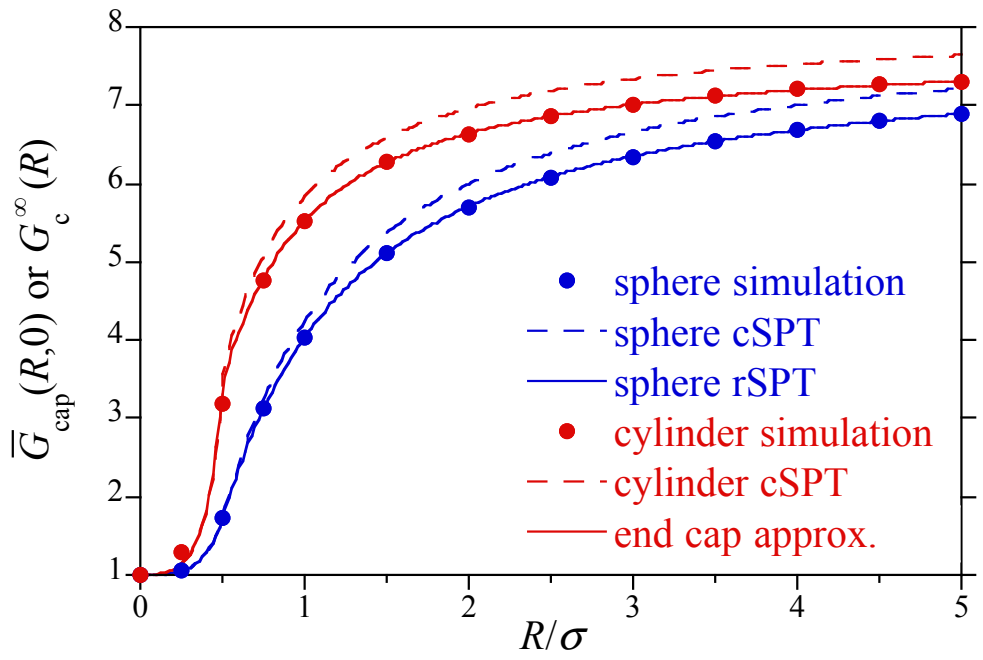
8
7
6
5
4
3
2
1
0
1
2
3
4
5
$\overline{G}_{cap}(R,0)$ or $G_c^{\infty}(R)$
R/σ
sphere simulation
sphere cSPT
sphere rSPT
cylinder simulation
cylinder cSPT
end cap approx.

Figure 2.

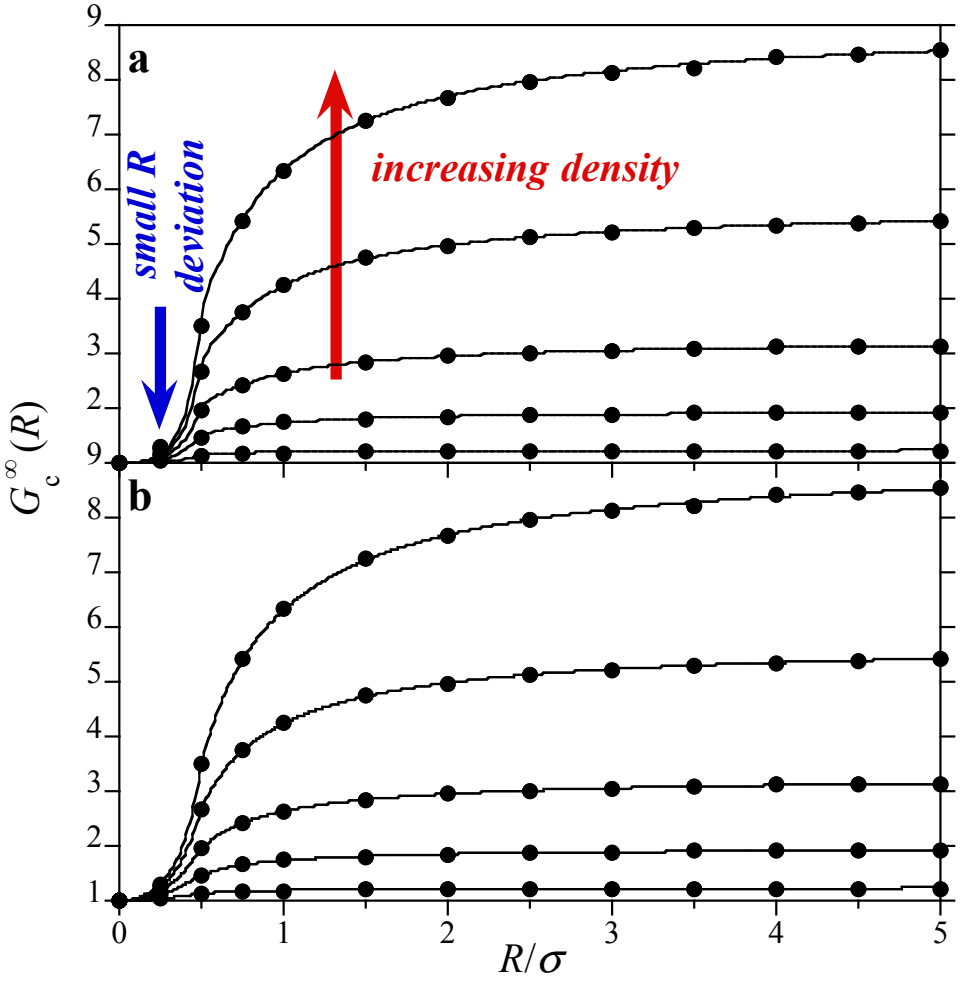
a
b
small R deviation
increasing density
$G_c^{\infty}(R)$
R/σ
0
1
2
3
4
5
1
2
3
4
5
6
7
8
9

Figure 3.

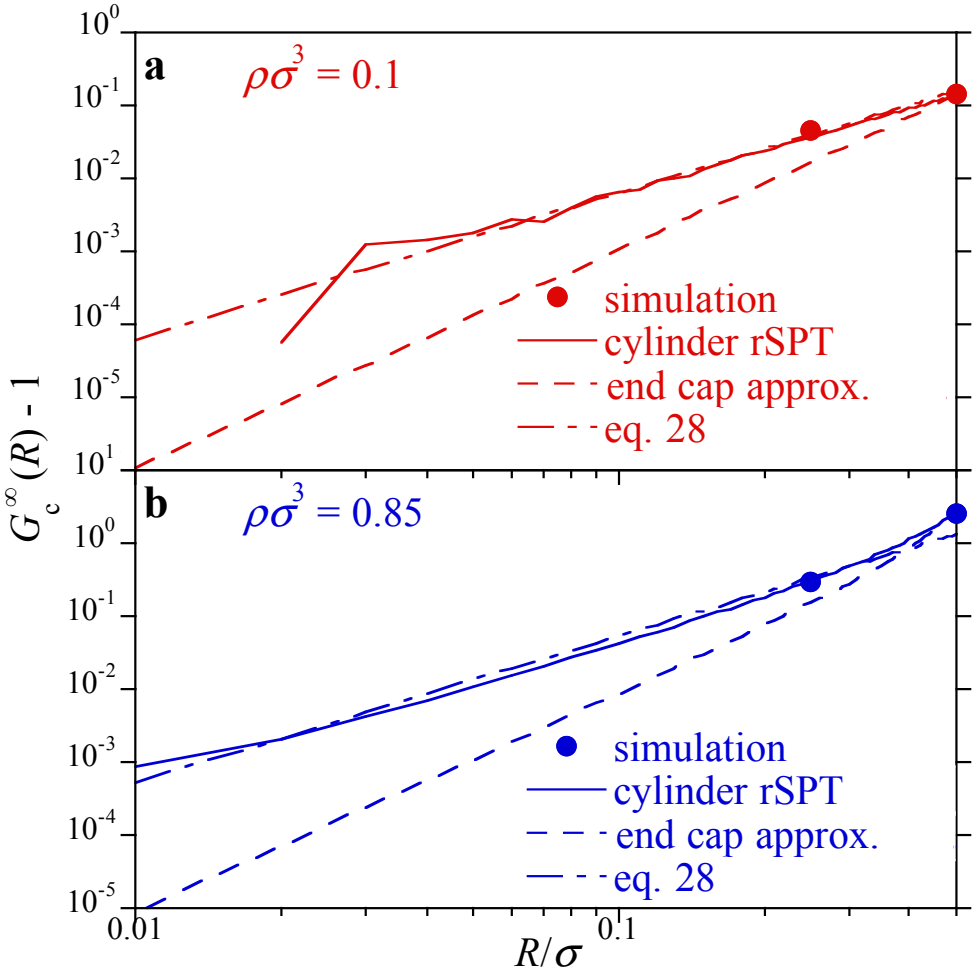
a
$\rho\sigma^3 = 0.1$
simulation
cylinder rSPT
end cap approx.
eq. 28
b
$\rho\sigma^3 = 0.85$
simulation
cylinder rSPT
end cap approx.
eq. 28
$G_c^{\infty}(R) - 1$
R/σ
10^0
10^{-1}
10^{-2}
10^{-3}
10^{-4}
10^{-5}
10^1
0.01
0.1

Figure 4.

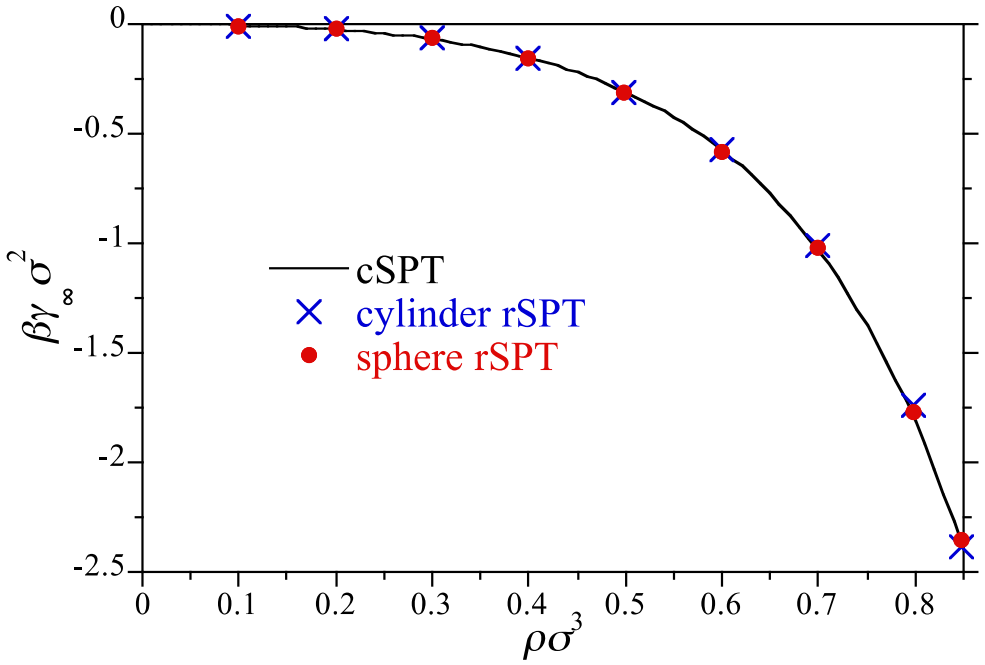
0
-0.5
-1
-1.5
-2
-2.5
0
0.1
0.2
0.3
0.4
0.5
0.6
0.7
0.8
$\beta\gamma_\infty\sigma^2$
$\rho\sigma^3$
cSPT
cylinder rSPT
sphere rSPT

Figure 5.

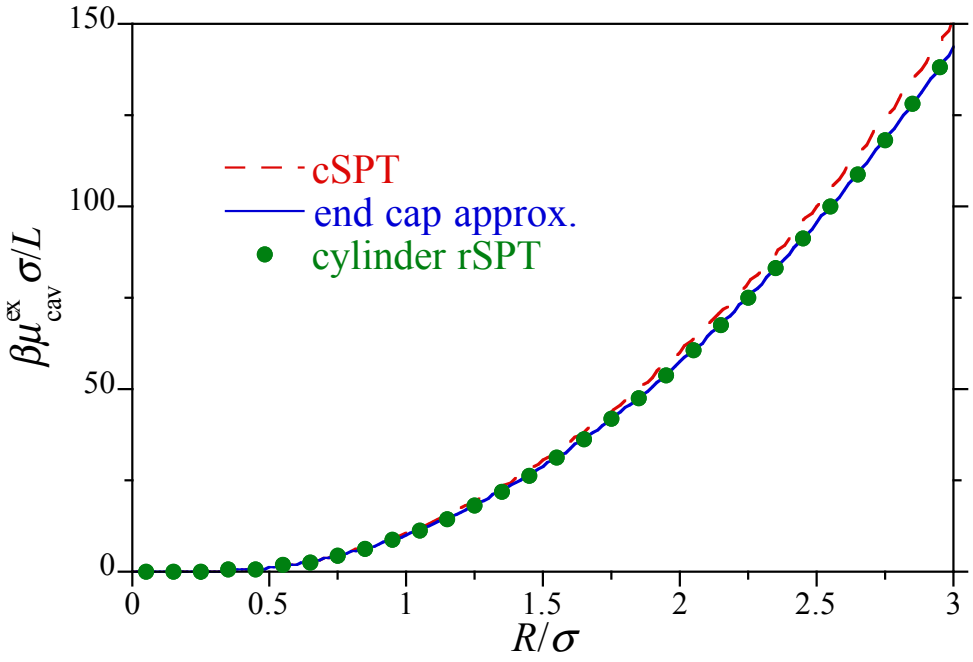
150
100
50
0
0
0.5
1
1.5
2
2.5
3
cSPT
end cap approx.
cylinder rSPT
$\beta\mu^{ex}_{cav}\sigma/L$
R/σ

Figure 6.

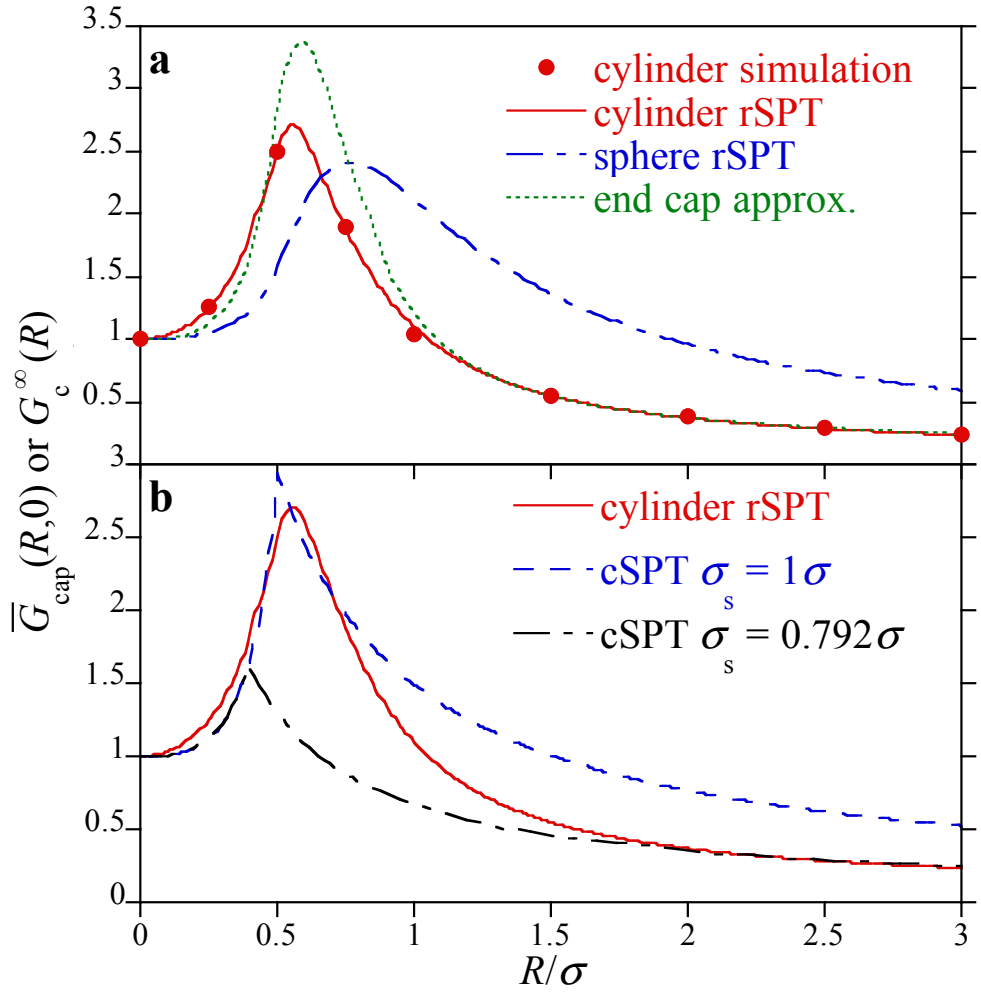
a
b
cylinder simulation
cylinder rSPT
sphere rSPT
end cap approx.
cylinder rSPT
cSPT $\sigma_s = 1\sigma$
cSPT $\sigma_s = 0.792\sigma$
$\overline{G}_{cap}(R,0)$ or $G_c^{\infty}(R)$
R/σ
0
0.5
1
1.5
2
2.5
3
3.5

Figure 7.

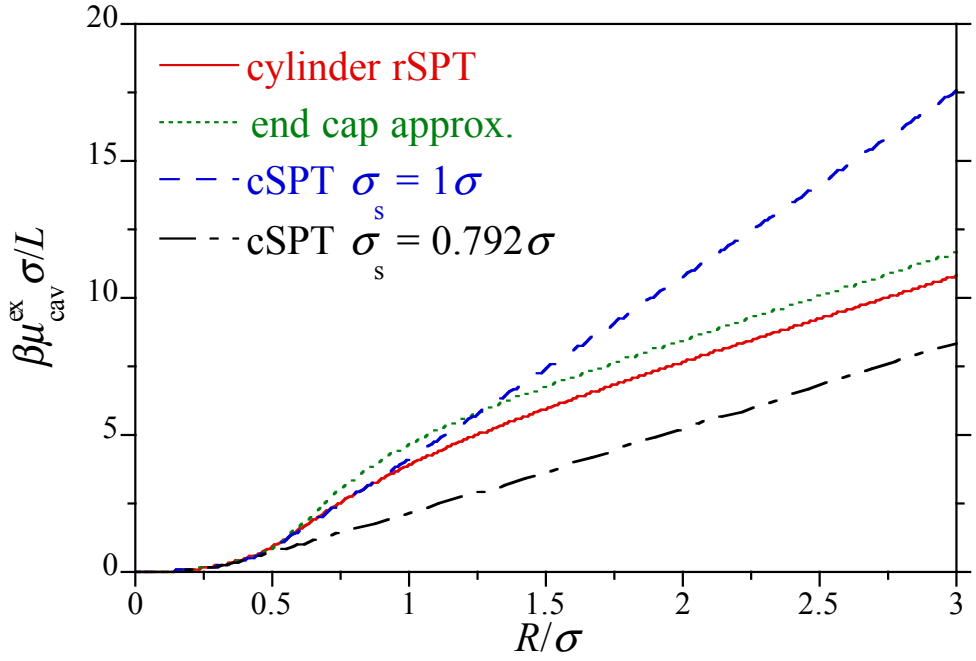
cylinder rSPT
end cap approx.
cSPT $\sigma_s = 1\sigma$
cSPT $\sigma_s = 0.792\sigma$
$\beta\mu_{cav}^{ex}\sigma/L$
R/σ
0
5
10
15
20
0
0.5
1
1.5
2
2.5
3

Figure 8.

References

[1] H. Reiss, H. L. Frisch, and J. L. Lebowitz, J. Chem. Phys. **31**, 369 (1959).

[2] H. Reiss, H. L. Frisch, E. Helfand, and J. L. Lebowitz, J. Chem. Phys. **32**, 119 (1960).

[3] H. Reiss, Adv. Chem. Phys. **9**, 1 (1965).

[4] R. A. Pierotti, J. Phys. Chem. **69**, 281 (1965).

[5] R. A. Pierotti, Chem. Rev. **76**, 717 (1975).

[6] A. Ben-Naim and H. L. Friedman, J. Phys. Chem. **71**, 448 (1967).

[7] F. H. Stillinger, J. Soln. Chem. **2**, 141 (1973).

[8] J. R. Henderson, J. Chem. Phys. **116**, 5039 (2002).

[9] J. R. Henderson and F. van Swol, J. Chem. Phys. **89**, 5010 (1988).

[10] F. M. Floris, J. Phys. Chem. B **108**, 16244 (2004).

[11] H. S. Ashbaugh and T. M. Truskett, J. Chem. Phys. **134**, 10, 014507 (2011).

[12] H. S. Ashbaugh and L. R. Pratt, Rev. Mod. Phys. **78**, 159 (2006).

[13] J. R. Dowdle, S. V. Buldyrev, H. E. Stanley, P. G. Debenedetti, and P. J. Rossky, J. Chem. Phys. **138**, 12, 064506 (2013).

[14] H. S. Ashbaugh, J. Chem. Phys. **130**, 8, 204517 (2009).

[15] H. S. Ashbaugh and L. R. Pratt, J. Phys. Chem. B **111**, 9330 (2007).

[16] H. S. Ashbaugh, Chem. Phys. Lett. **477**, 109 (2009).

[17] R. M. Gibbons, Mol. Phys. **17**, 81 (1969).

[18] R. M. Gibbons, Mol. Phys. **18**, 809 (1970).

[19] J. A. Barker and J. R. Henderson, Rev. Mod. Phys. **48**, 587 (1976).

[20] G. Lasher, J. Chem. Phys. **53**, 4141 (1970).

[21] M. A. Cotter, Phys. Rev. A **10**, 625 (1974).

[22] A. G. Ogston, Trans. Faraday Soc. **54**, 1754 (1958).

[23] L. R. Pratt and A. Pohorille, Proc. Natl. Acad. Sci. U. S. A. **89**, 2995 (1992).

[24] A. Jain and H. S. Ashbaugh, J. Chem. Phys. **129**, 8, 174505 (2008).

[25] G. Graziano, J. Phys. Chem. B **113**, 11232 (2009).

[26] G. Graziano, Chem. Phys. Lett. **440**, 221 (2007).

[27] H. Hadwiger, *Vorlesungen u□ber Inhalt, Oberfla□che und Isoperimetrie* (Springer, Berlin, 1957).

[28] P. M. Konig, R. Roth, and K. R. Mecke, Phys. Rev. Lett. **93**, 4, 160601 (2004).

[29] R. Roth, Y. Harano, and M. Kinoshita, Phys. Rev. Lett. **97**, 4, 078101 (2006).

[30] B. B. Laird, A. Hunter, and R. L. Davidchack, Phys. Rev. E **86**, 5, 060602 (2012).

[31] F. Sedlmeier and R. R. Netz, J. Chem. Phys. **137**, 14, 135102 (2012).

[32] H. Hansen-Goos and R. Roth, J. Phys. Cond. Matt. **18**, 8413 (2006).

[33] Z. H. Jin, J. Kim, and J. Z. Wu, Langmuir **28**, 6997 (2012).

[34] S. M. Oversteegen and R. Roth, J. Chem. Phys. **122**, 214502 (2005).

[35] D. W. Siderius and D. S. Corti, Phys. Rev. E **71**, 12, 036141 (2005).

[36] D. W. Siderius and D. S. Corti, Phys. Rev. E **75**, 21, 011108 (2007).

[37] T. M. Reed and K. E. Gubbins, *Applied Statisitcal Mechanics: Thermodynamics and Transport Properties of Fluids* (Butterworth-Heinmann, Boston, 1973).

[38] C. Benzi, M. Xossi, R. Improta, and V. Barone, J. Comp. Chem. **26**, 1096 (2005).

[39] D. Frenkel and B. Smit, *Understanding Molecular Simulation: From Algorithms to Applications* (Academic Press, San Diego, 2001), second edn.

[40] J. K. Percus, J. Stat. Phys. **15**, 423 (1976).

[41] G. Hummer, S. Garde, A. E. Garcia, M. E. Paulaitis, and L. R. Pratt, J. Phys. Chem. B **102**, 10469 (1998).

[42] J. R. Henderson and F. van Swol, Mol. Phys. **51**, 991 (1984).

[43] P. Attard and G. A. Moule, Mol. Phys. **78**, 943 (1993).

[44] M. Heying and D. S. Corti, Mol. Phys. **112**, 2160 (2014).